Isospin symmetry in the *sd* shell: Transition strengths in the neutron-deficient *sd* shell nucleus ^{33}Ar

A. Wendt,[1] J. Taprogge,[1,2] P. Reiter,[1] P. Golubev,[3] H. Grawe,[4] S. Pietri,[4] P. Boutachkov,[5] A. Algora,[6,7] F. Ameil,[4] M. A. Bentley,[8] A. Blazhev,[1] D. Bloor,[8] B. S. Nara Singh,[8] M. Bowry,[9] A. Bracco,[10] N. Braun,[1] F. Camera,[10] J. Cederkäll,[3] F. Crespi,[10] A. de la Salle,[11] D. DiJulio,[3] P. Doornenbal,[12] K. Geibel,[1] J. Gellanki,[3] J. Gerl,[4] J. Grębosz,[13] G. Guastalla,[5] T. Habermann,[4] M. Hackstein,[1] R. Hoischen,[4] A. Jungclaus,[2] E. Merchán,[5] B. Million,[10] A. Morales,[10] K. Moschner,[1] Zs. Podolyák,[9] N. Pietralla,[5] D. Ralet,[5] M. Reese,[5] D. Rudolph,[3] L. Scruton,[8] B. Siebeck,[1] N. Warr,[1] O. Wieland,[10] and H. J. Wollersheim[4]

[1]*Institut für Kernphysik, Universität zu Köln, Köln, Germany*
[2]*Instituto de Estructura de la Materia, CSIC, Madrid, Spain*
[3]*Department of Physics, Lund University, Lund, Sweden*
[4]*Helmholtzzentrum für Schwerionenforschung GmbH (GSI), Darmstadt, Germany*
[5]*Institut für Kernphysik, Technische Universität Darmstadt, Darmstadt, Germany*
[6]*Instituto de Fisica Corpuscular, CSIC-Universidad de Valencia, Valencia, Spain*
[7]*Institute of Nuclear Research of the Hungarian Academy of Science, Debrecen, Hungary*
[8]*Department of Physics, University of York, York, United Kingdom*
[9]*Department of Physics, University of Surrey, Guildford, United Kingdom*
[10]*Dipartimento di Fisica, Università de Milano, and INFN Sezione Milano, Milano, Italy*
[11]*Department of Physics, University of Nantes, Nantes, France*
[12]*RIKEN Nishina Center, Wako, Saitama, Japan*
[13]*The Institute of Nuclear Physics PAN, Kraków, Poland*

(Received 10 April 2014; revised manuscript received 25 August 2014; published 4 November 2014; corrected 23 January 2015)

Reduced transition strengths of the deexciting transitions from the first two excited states in ^{33}Ar were measured in a relativistic Coulomb excitation experiment at the GSI Helmholtz center. The radioactive ion beam was produced by fragmentation of a primary ^{36}Ar beam on a ^{9}Be target followed by the selection of the reaction product of interest via the GSI Fragment Separator. The ^{33}Ar beam hit a secondary ^{197}Au target with an energy of approximately 145 MeV/nucleon. An array of high-purity germanium cluster detectors and large-volume BaF_2 scintillator detectors were employed for γ-ray spectroscopy at the secondary target position. The Lund-York-Cologne Calorimeter was used to track the outgoing ions and to identify the nuclear reaction channels. For the two lowest energy excited states of ^{33}Ar the reduced transition strengths have been determined. With these first results the $T_z = -3/2$ nucleus ^{33}Ar is now, together with ^{21}Na ($T_z = -1/2$), the only neutron-deficient odd-A *sd* shell nucleus in which experimental transition strengths are available. The experimental values are compared to results of shell-model calculations which describe simultaneously mirror-energy differences and transition-strength values of mirror pairs in the *sd* shell in a consistent way.

DOI: 10.1103/PhysRevC.90.054301 PACS number(s): 21.10.Hw, 23.20.Js, 25.70.De, 27.30.+t

I. INTRODUCTION

The *sd* shell between ^{16}O and ^{40}Ca provides an excellent study ground for the intriguing interplay of drip-line effects, isospin symmetry distortion, and monopole-driven shell evolution. Moreover, the neutron-deficient side is of high relevance for the astrophysical rapid proton capture process path. Experiments with radioactive ion beams allowed us to investigate the low-lying excited states of the $|T_z| \leqslant 2$ *sd* shell nuclei [1,2]. A sensitive observable for these neutron-deficient nuclei is given by the energy differences between excited states of so-called mirror nuclei with $T_z = \pm T$. The "mirror-energy difference" (MED) is defined as $\mathrm{MED(I)} = E_x(I, T_z = -T) - E_x(I, T_z = +T)$ [3,4]. In fact, the investigation of isobaric nuclei allows a very detailed test of effective shell-model interactions in order to reproduce the increasing amount of experimental data.

An exceptionally large MED value was found for the 2^+ states in the mirror pair ^{36}Ca-^{36}S [1]. Previous shell-model calculations in this region were based on the original isospin symmetric USD interaction [5]. In order to describe the new results from the mirror pair ^{36}Ca-^{36}S, a modified USD version, the USD_1^m interaction [1] was introduced. This interaction, here named USD_1^m, keeps the isospin symmetry in the two-body matrix elements (TBMEs) but includes monopole corrections to the original USD [6]. However, the single-particle energies (SPEs) are isospin dependent, because the experimental excitation energies of ^{17}O and ^{17}F are used. This interaction was employed to reproduce all MED values of $T = 1,2$ *sd* shell mirror pairs. While the mirror-energy differences of most nuclei are reasonably well reproduced, the MED values for $A = 30,32$ as well as those for $A = 18,24$ differ substantially from the experimental results (see the black curve in Fig. 1). Thus, additional empirical modifications of the interaction were introduced [1] which were different for the lower mass and higher mass triangles in the *sd* shell, here referred to as USD_2^m and USD_3^m, respectively (see Sec. III). The new findings concur with a reduction of the $N = 14$ shell gap in neutron-deficient nuclei close to $Z = 20$ at the proton drip line and a similar reduction for the $Z = 14$ gap (close to $N = 8$).

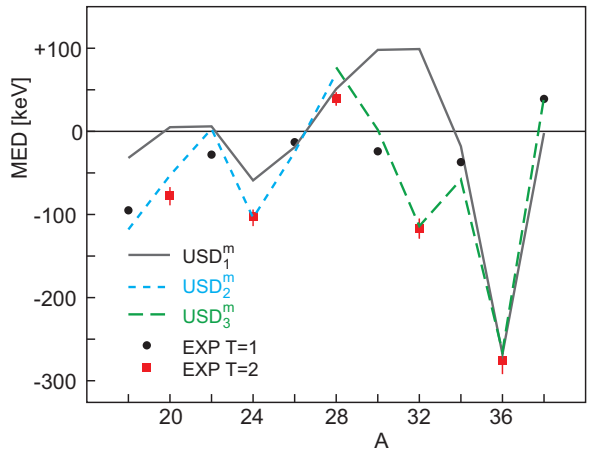

FIG. 1. (Color online) Experimental MED values (2_1^+ states) of $T_z = \pm 1$ (black dots) and $T_z = \pm 2$ (red squares) *sd* shell nuclei with shell-model calculations employing different interactions (different lines). For details see the text.

The calculations are in good agreement with the observed $T = 2$, $J = 2^+$ MED value (see Fig. 1). The results of the modifications were experimentally supported by a subsequent result [2] for the ^{20}Mg and ^{20}O mirror pair.

The $T = \frac{3}{2}$ mirror pairs are now in the focus to verify the validity of the isospin violating interaction and to provide a refined test due to the implications of the unpaired nucleon. At this point not only the experimental $T = \frac{3}{2}$ MED values for the single-particle/hole states are compared to the values obtained with the modified interaction. Also the isospin-dependent reduced transition strengths in mirror pairs have to be reproduced in a consistent picture. Here a more stringent and refined test of theory is given by the isoscalar (IS) and isovector (IV) $E2$ matrix elements (MEs) for *sd* shell $T = 1,2,3/2$ nuclei which are extracted from $B(E2; 2_1^+ \rightarrow 0_1^+)$ values for $T = 1,2$ pairs and from $B(E2; \frac{5}{2}_1^+, \frac{3}{2}_1^+ \rightarrow \frac{1}{2}_1^+)$ values for $T = \frac{3}{2}$ pairs.

Experimental $B(E2)$ values are available for all $T_z = 1, \frac{3}{2}$ and all even-even $T_z = 2$ nuclei at or close to the valley of stability. For the neutron-deficient partners, the situation is quite different: only three out of five $T_z = -2$ experimental $B(E2)$ values are available and for none of the ten $T_z = -\frac{3}{2}$ nuclei is a transition strength value known. The $T = 1,2$ $B(E2; 2_1^+ \rightarrow 0_1^+)$ values due to seniority change by $\Delta v = 2$ are dominated by large isoscalar matrix elements and exhibit collective features towards mid-(sub)shell by coherent superposition of proton and neutron contributions. On the other hand transitions between $T = 3/2$ states with different nucleons coupled to identical even-even intrinsic configurations will show single-particle character and sensitivity to subshell gaps. The latest results from γ-spectroscopy experiments are available for excited states in the $T_z = -\frac{3}{2}$ even-odd nuclei ^{25}Si and ^{29}S [7]. From these measurements, however, indirect evidence is found that the first two excited states in ^{25}Si and ^{29}S are rotational excitations of the ground state. Shell-model calculations provide predictions for increased $B(E2)$ values. The expectation of collective behavior of neutron-deficient *sd* shell nuclei can be verified by measuring directly the reduced transition strengths.

The intriguing cases are obviously $A = 25,29$ from the theory point of view as they comprise the subshell magic numbers $Z,N = 14,16$. However, the Coulomb excitation experiments are hampered for the following reasons. The ground state configuration of ^{25}Si and ^{29}S is $I = \frac{5}{2}^+$, implying a reduced cross section for Coulomb excitation as compared to the $I = \frac{1}{2}^+$ ground state of ^{33}Ar. Moreover the relevant $\frac{3}{2} \rightarrow \frac{1}{2}$ $E2$ transition cannot be extracted. Both objections are circumvented for $A = 33$, which therefore is the best case for a pilot experiment.

Energies of excited states in ^{33}Ar are established up to 3.819 MeV. A first experiment populated excited states in ^{33}Ar by the ^{36}Ar(^{3}He,^{6}He)^{33}Ar transfer reaction, employing a 70 MeV ^{3}He beam from the Michigan State University (MSU) cyclotron [8]. The second experiment exploited a 150 MeV/nucleon ^{36}Ar beam at MSU to produce a beam of ^{34}Ar, and excited states in ^{33}Ar were studied after neutron removal reactions [9]. The spin-parity assignments of even-parity states of ^{33}Ar are proposed, whereas no lifetime information of excited states or transition strength values is available. Its mirror, the close-to-stability nucleus ^{33}P, has been studied extensively via γ-ray spectroscopy in the past [10–16].

II. EXPERIMENTAL SETUP AND DATA ANALYSIS

The GSI-PreSpec setup was employed to determine the transition strengths of excited states in ^{33}Ar. A primary beam of ^{36}Ar was provided by the heavy-ion synchrotron SIS with an energy of 450 MeV/nucleon. The beam particles hit the primary ^{9}Be production target with a thickness of 4 g/cm^2 at the entrance of the Fragment Separator (FRS) [17]. The average primary beam intensity was 5×10^9 ions/s. The ^{33}Ar fragments of interest were selected in flight on an event-by-event basis using the FRS in its achromatic mode [17]. In total 1.3×10^9 ^{33}Ar ions have been identified by the FRS detectors, impinging at an average rate of 1.5×10^4 ions/s on the 386 mg/cm^2 secondary ^{197}Au target at an energy of 145 MeV/nucleon.

A subset of the RISING γ-ray detectors surrounded the secondary target position [18]. The detector assembly consisted of 15 high-purity germanium (HPGe) EUROBALL cluster detectors [19], containing seven large-volume Ge crystals each. The cluster detectors were positioned in two rings at extreme forward angles of 16° and 36°. In addition the HECTOR array [20], comprising eight large volume BaF_2 detectors, was exploited for the detection of high-energetic γ rays with very good timing resolution.

The outgoing beam particles and reaction products were tracked and identified behind the secondary target using the newly developed Lund-York-Cologne Calorimeter (LYCCA) [21]. The main parts of this detector array are twelve Si-CsI(Tl) detector modules used as a ΔE-E detector telescope. These detector modules are positioned at a distance of 3.4 m downstream behind the target. A position sensitive double-sided Si detector (DSSD) is mounted very closely behind the secondary Au target. Two ultrafast plastic scintillator

detectors [22] are used to measure the time of flight (ToF) of the outgoing particles. One plastic detector is mounted close to the target, the second detector in front of the ΔE-E detector telescopes. The energy loss in the DSSDs, the total kinetic energy deposition in CsI(Tl) scintillators, and the time-of-flight measurement by the plastic scintillator provide Z and A identification behind the secondary target. The tracking of scattered particles is based on position-sensitive time projection chambers (TPCs) in front of the secondary target, the position sensitive DSSD close to the target position, and the Si strip detectors of the twelve LYCCA detector modules. Tracking is needed for the scattering angle determination and for a precise Doppler correction. A precise determination is made of the γ-ray emission angle with respect to the fast moving nuclei, and a velocity measurement is obtained. A Doppler correction is performed in order to reduce the Doppler broadening and to obtain the best possible energy resolution for the γ rays emitted by ions moving at relativistic velocities.

The analysis of this experiment is based on event-by-event correlations between signals from particle and γ-ray detectors. Ion identification before and after the target is used to reject the nuclear reaction channels and to select the ions of interest after Coulomb excitation. The FRS detectors are employed for tracking and identification of the ions passing through the separator up to the secondary target position. The analysis of the FRS detectors follows closely the description given in [17]. From LYCCA all information related to the outgoing particles is obtained. The average velocity of the ions along the LYCCA flight path is deduced from the time-of-flight measurement. The trajectory after the secondary target is calculated from the pixel position of the target DSSD and the ΔE-E modules. Additional information from the energy loss in the target DSSD is exploited to measure the charge of the outgoing particle. The ΔE-E modules stop the particles. From the energy loss in the DSSDs the charge is deduced again to exclude events with reactions in the detector assembly. The remaining kinetic energy is deposited in the CsI crystals.

The combined information of LYCCA and FRS detectors allows improved and redundant ToF measurement between all LYCCA detectors and the timing signal of the S4 scintillator. Three position measurements are combined for the scattering angle determination. The two TPC detectors in front of the secondary target provide the angles of the ions relative to the central beam axis. The position at the secondary Au target is measured. The LYCCA Z identification is illustrated in Fig. 2 where the total kinetic energy vs the energy loss of an ion in the DSSD is shown.

The mass resolving power is illustrated in Fig. 3 for the case of the ^{30,31}S isotopes, which are produced in the secondary target by fragmentation of incoming ^{33}Ar ions. For this plot a two-dimensional gate was set on the $Z = 16$ isotopes in the LYCCA ΔE-E plot (cf. Fig. 2). A mass resolution of $\frac{\Delta A}{A} = 0.019(2)$ (FWHM) is obtained in the $A \approx 30$ region. This value is in good agreement with a LYCCA mass resolution of $\frac{\Delta A}{A} = 0.006$–$0.018$ for nuclei in the region $A \approx 60$–80 [21]. Consequently, neighboring isotopes in the region of ^{33}Ar are separated unambiguously.

The main γ-ray detectors were the cluster detectors, of which fourteen were operational during the experiment. The

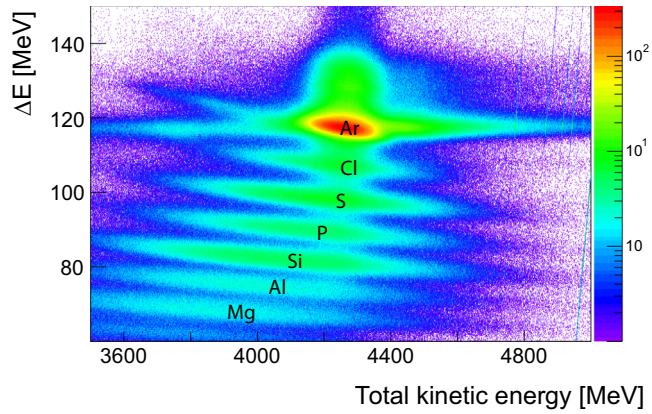

FIG. 2. (Color online) ΔE-E plot of the LYCCA for Z identification.

analysis of the information obtained from the cluster detectors utilizes an add-back algorithm which applies for events with energy depositions in more than one crystal of a cluster detector. For the Doppler correction, the angle between the germanium crystal and the flight path of the ion is calculated from the position of the hit crystal. The γ rays, originating from prompt deexcitations at the secondary target, are selected by a prompt time gate. Background radiation is subtracted. The energy resolution for the in-beam measurement was 2.5% for a transition energy of 1.9 MeV and mainly caused by Doppler broadening. The γ-ray spectra obtained for the ^{36}Ar and the ^{33}Ar isotopes are shown in Fig. 4. The different width of the peaks at 1360(3) and 1804(6) keV from ^{33}Ar are expected due to incomplete Doppler correction and differing half lives for the two transitions. Using experimental and shell-model $E2$ strength values the half-lives are 1.75/2.05 ps for the $3/2^+$ state and 0.79/0.81 ps for the $5/2^+$ state. The moderate ^{36}Ar broadening could be explained by the differing kinematics and/or fragmentation for beam particles and the short half-life of 0.33 ps with respect to the flight time within the Au target.

The reduced transition strengths were determined for the two lowest excited states in ^{33}Ar at 1359 and 1798 keV relative

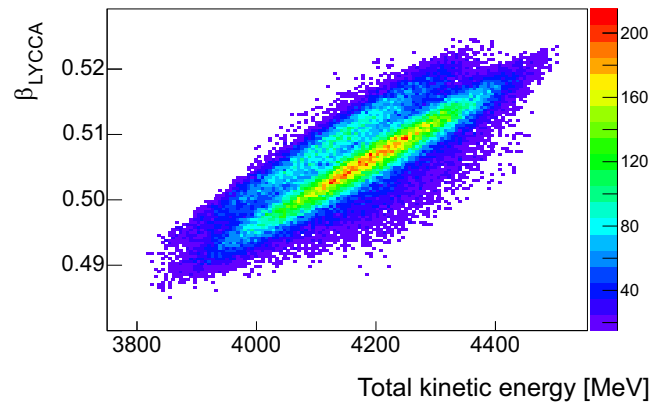

FIG. 3. (Color online) β-E plot of the LYCCA, which is used for mass identification, demonstrated for ^{31,30}S produced in second fragmentation of ^{33}Ar (see text).

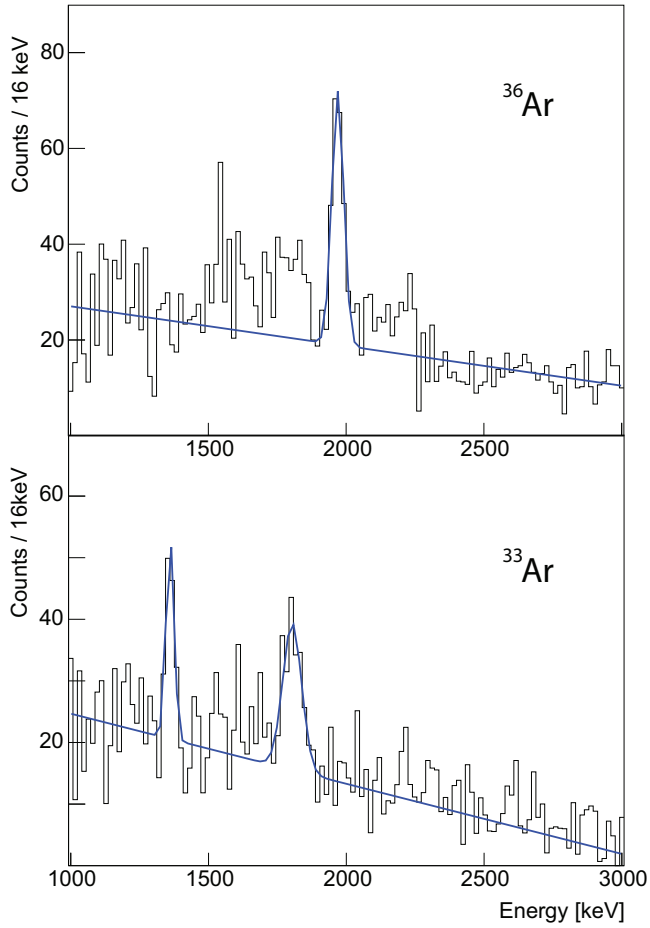

FIG. 4. (Color online) Background-subtracted, Doppler-corrected γ-ray spectra showing the $2_1^+ \rightarrow 0^+$ transition at 1970(3) keV from ^{36}Ar in the top panel, and the $(\frac{3}{2})^+ \rightarrow (\frac{1}{2})^+$- at 1360(3) keV and the $(\frac{5}{2})^+ \rightarrow (\frac{1}{2})^+$ transitions at 1804(6) keV from ^{33}Ar in the bottom panel.

to the known $B(E2)$ value of the pure $E2$ transition, $2_1^+ \rightarrow 0^+$, with an energy of 1970 keV from ^{36}Ar. The comparison is based on the Coulomb excitation cross sections deduced from the number of detected γ rays for ^{36}Ar and ^{33}Ar, the number of reaction centers in the secondary target, and the number of ions impinging on the target measured by the particle detectors. The energy-dependent γ-ray detection efficiency takes into account that the γ rays are emitted from a fast moving source with $\beta \approx 0.57$. Different γ-ray detection efficiencies (caused by differing γ-ray energies and ion velocities) have been taken into account. In this way the Coulomb cross section values are deduced from the experimental data. More details can be found in Ref. [23].

The reduced transition strengths are determined from the total Coulomb cross section employing the computer program DWEIKO [24]. For ^{36}Ar, Coulomb excitation of the first excited 2_1^+ state is dominating. However, also the transition $0^+ \rightarrow 3_1^-$ and its small impact on the population of the 2_1^+ state by an $E1$ decay is taken into account for the determination of the $B(E2, 2^+ \rightarrow 0^+)$ value. The $B(E2)$ value of the first excited state in ^{36}Ar has been measured over several decades by various experimental techniques, and the adopted value of $B(E2; 2_1^+ \rightarrow 0^+) = 8.5(8)$ W.u. of Refs. [25,26] is used.

TABLE I. Gamma-ray energies (keV) and $B(E2)$ values (W.u.) for ^{36}Ar and ^{33}Ar. Literature values are taken from Refs. [25,26].

	^{36}Ar	^{33}Ar	
	$2^+ \rightarrow 0^+$	$\frac{3}{2}^+ \rightarrow \frac{1}{2}^+$	$\frac{5}{2}^+ \rightarrow \frac{1}{2}^+$
$\text{Energy}_{\text{Lit}}$	1970.38(5)	1359(2)	1798(2)
$\text{Energy}_{\text{Exp}}$	1970(3)	1360(3)	1804(6)
$B(E2)_{\text{Lit}}$	8.5(8)		
$B(E2)_{\text{Exp}}$		6.4(15)	5.8(16)

The determination of the two values $B(E2; (\frac{5}{2})_1^+ \rightarrow (\frac{1}{2})_{g.s.}^+)$ and $B(E2; (\frac{3}{2})_1^+ \rightarrow (\frac{1}{2})_{g.s.}^+)$ for ^{33}Ar from the γ-ray transitions takes into account the two decay branches of the $(\frac{5}{2})_1^+$ state. A small branching ratio of $b = 2.34(40)\%$ was measured directly by an in-beam γ-ray spectroscopy experiment [9]. The final results are given in Table I.

III. RESULTS AND DISCUSSION

The results of shell-model calculations, which include the modifications explained in the introductory part of this paper and in Ref. [1], are compared to experimental level energies, namely MED values, and $B(E2)$ values for sd shell mirror nuclei. The following modifications were done: (*i*) For $A \leqslant 28$, the $\pi 0d_{5/2}$ single-particle energy was increased by 200 keV and the $\pi(0d_{5/2},0d_{5/2})$ two-body matrix elements were quenched by the factor 0.95 (USD_2^m). (*ii*) For $A > 28$, the $\pi 0d_{5/2}$ SPE was reduced by 300 keV and the $\nu 0d_{5/2}$ SPE was increased by 900 keV (USD_3^m). The main goal is to reproduce simultaneously the excitation energies of the $T_z = -\frac{3}{2}$ sd shell nuclei as well as the reduced transition strengths. To avoid distortion by deformed structure in mid-shell and to stress single-particle character, the $T = 3/2$ states were selected according to their shell-model structure and experimentally at excitation energies well below the 2^+ states in the neighboring even-even nucleus. This restricts comparison to $d_{5/2}$-$s_{1/2}$ and $d_{3/2}$-$s_{1/2}$ pairs in the lower and upper shell, respectively. Experimental data for the MED values of $T_z = \pm\frac{3}{2}$ nuclei are shown in Fig. 5 for the lowest sd single-particle/hole states, i.e., $s_{1/2}$-$d_{5/2}$ in the lower part and $s_{1/2}$-$d_{3/2}$ in the upper part of the shell. The MED values are given disregarding which state is the ground state or whether it has particle or hole character. As transfer data are not accessible consistently, the particle/hole character was inferred from the shell-model wave functions.

Obviously the single-particle/hole MED values are more sensitive to structure effects than the 2^+ MED values for $T = 1,2$ shown in Fig. 1. The size of the experimental MED effect is in most cases far beyond Coulomb corrections including the Thomas-Ehrmann shift. The calculated MED values for the $A = 33$ pair of -203 keV for the $3/2^+$ state and -198 keV for the $5/2^+$ state should be compared with experimental values of $-73(2)$ keV and $-50(2)$ keV, respectively. The

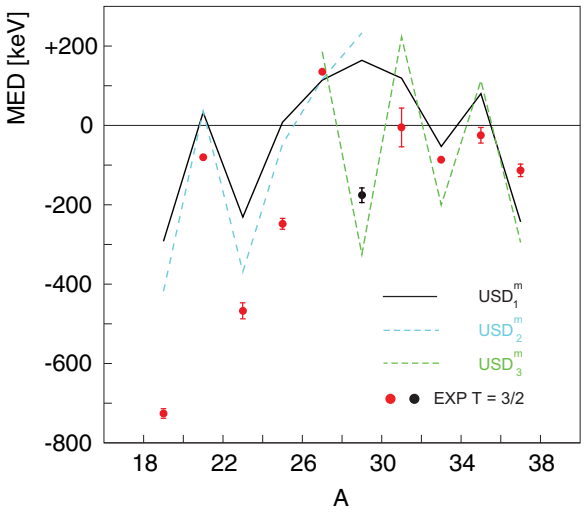

FIG. 5. (Color online) Experimental mirror energy differences of the first excited states of the $T = \frac{3}{2}$ *sd* shell mirror pairs and shell-model calculations [1]. The black dot indicates a new data point at $A = 29$; a measurement that was released in Ref. [7] after the modified USD$^m_{2,3}$ interactions were published in Ref. [1]. The experimental data, beside the $A = 29$ data point, are taken from [28].

odd-proton–odd-neutron staggering in the $T = 3/2$ MED values, besides the alternating proton/neutron valence nucleon coupled to a paired neutron/proton core, is due to the different shell gaps and/or single-particle/hole energies for protons and neutrons, respectively. This effect is qualitatively suggested in the USD$^m_1$ calculations. The effect is underestimated in the lower *sd* shell and overestimated in the upper *sd* shell. This does not reproduce the new experimental data point from [7] at $A = 29$. The USD$^m_{2,3}$ interactions clearly correct for the deviation at mid-shell and show an improved overall agreement with the experimental MED data, which legitimates again the changes. The damped staggering beyond $A = 30$ is not reproduced quantitatively in theory. In the lower shell the $d_{5/2}$-$s_{1/2}$ MEDs are sensitive to the $Z, N = 14$ subshell, while in the upper shell the $d_{3/2}$-$s_{1/2}$ MEDs are sensitive the $Z, N = 16$ subshell, which remained unchanged in the modified interaction.

In the following, the comparison between experimental results and the USD$^m_{2,3}$ calculation is extended in order to investigate transition strengths in these nuclei, too. $E2$ transition strengths were calculated with standard *sd* shell effective operators for the polarization charge $\Delta e^{\pi,\nu} = 0.35e$ [27].

The available experimental information on transition strengths in nuclei close to the $N = Z$ line is compared to results of shell-model calculations. All known $B(E2, 2^+ \rightarrow 0^+)$ values of even-even $T_z = \pm 1, \pm 2$ *sd* shell nuclei are shown in Fig. 6 . Due to the identical underlying structure, the transition strengths from these states to the ground state can be directly compared. In addition the results of shell-model calculations are displayed. In all plots of this type the blue (neutron-deficient) and red (neutron-rich) lines represent the results of the shell-model calculation with the USD$^m_{2,3}$ (USD$^m_2$ for $A \leqslant 28$, USD$^m_3$ for $A > 28$) interactions. The experimental data are marked by the blue (neutron-deficient) and red (neutron-rich) dots.

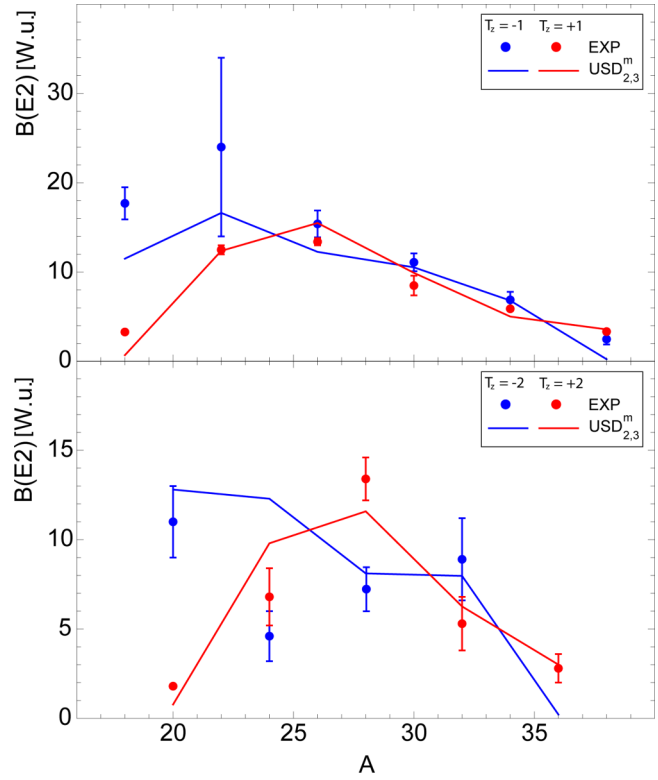

FIG. 6. (Color online) Experimental $B(E2)$ values (dots) and results from shell-model calculations (lines) are compared for $T_z = \pm 1, \pm 2$ *sd* shell nuclei. For details see text.

For $T_z = \pm 1$ pairs, the transition strengths of all *sd* shell nuclei are well known despite the ^{22}Mg value, which has a large uncertainty $B(E2; 2^+_1 \rightarrow 0^+_1) = 24(10)$ W.u. [28]. The calculated $B(E2)$ values are in good agreement with the experimental data. Only in the case of ^{26}Si do larger discrepancies occur between the different interactions. The determination of $B(E2)$ values for the highly exotic $T_z = -2$ nuclei is experimentally very challenging. For the neutron-deficient nucleus ^{36}Ca no transition strengths are known. The transition strengths of ^{20}Mg [29] and ^{32}Ar [30] and those of all neutron-rich nuclei are in good agreement with the shell-model calculations. The $B(E2)$ value of ^{24}Si [31] shows a significant deviation between experiment and theory. On the other hand the recently measured value for ^{28}S [32] excellently corroborates the shell-model prediction.

The available information on transition strengths for the neutron deficient partner of $T_z = \pm\frac{3}{2}$ mirror pairs is limited to our newly measured values, which are summarized in Table II together with the results of the shell-model calculations. The experimental values for ^{33}P are taken from a lifetime measurement employing the Doppler-shift-attenuation method, published in Refs. [14,15]. The $T_z = \pm\frac{3}{2}$ mirror pairs separate in two groups: one with an unpaired neutron in the proton-rich partner and another one with an unpaired proton. Nuclei of these groups differ largely in their proton separation energies (S_p). The unpaired proton is less bound than a paired proton. Therefore no excited states below S_p exist in the nuclei with an unpaired proton.

TABLE II. $B(E2)$ values from experiments and shell-model calculations, given in Weisskopf units; experimental data for ^{33}P are taken from Refs. [14] (left column) and [15] (right column).

Nucl.	$J_i \to J_f$	USD$_1^m$	USD$_3^m$	Exp. data	
^{33}Ar	$\frac{3}{2} \to \frac{1}{2}$	5.013	4.790	6.4(15)	
	$\frac{5}{2} \to \frac{1}{2}$	6.684	6.225	5.8(16)	
	$\frac{5}{2} \to \frac{3}{2}$	1.550	1.410		
^{33}P	$\frac{3}{2} \to \frac{1}{2}$	5.916	5.827	10(4)	8.1(24)
	$\frac{5}{2} \to \frac{1}{2}$	4.932	4.658	5.1(8)	4.8(6)
	$\frac{5}{2} \to \frac{3}{2}$	0.809	0.797	<24	<37

For $T_z = \pm\frac{3}{2}$ mirror pairs two different excited states, like the $(\frac{5}{2})^+$ and the $(\frac{3}{2})^+$ states in ^{33}Ar, deexcite directly by γ-ray emission to the ground state. Furthermore, the proton separation energies are well below 1 MeV for nuclei with an unpaired proton. In the neutron-deficient partners the energies of excited states are larger than the proton separation energies. Thus, shell-model comparisons are limited to mirror pairs with an unpaired neutron in the neutron-deficient partner. Transition strengths of all neutron-rich partners are available, but not a single $B(E2)$ value for the neutron deficient partners was known prior to our study. The two new transition strengths values for ^{33}Ar allow a first comparison with results from the neutron-rich nucleus ^{33}P. Together with the values of the shell-model calculations, all the findings are shown in Fig. 7.

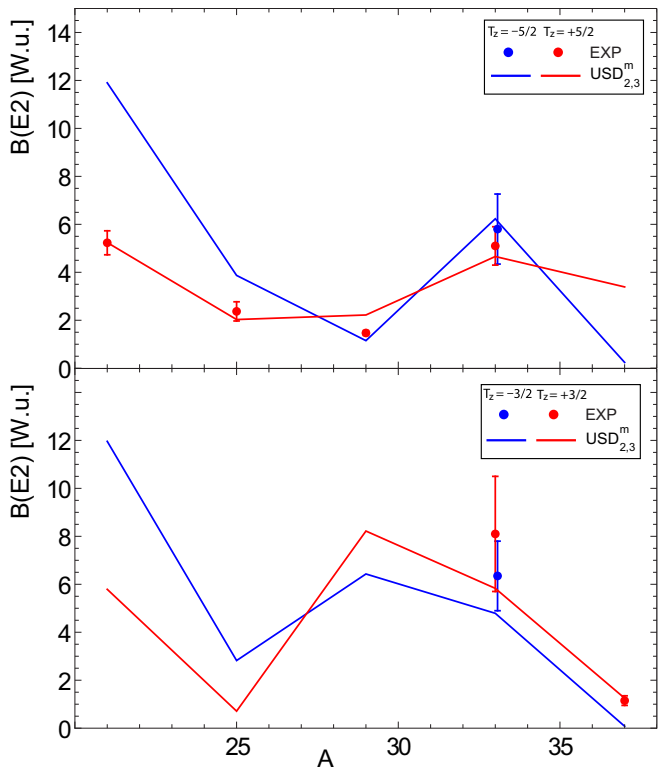

FIG. 7. (Color online) Experimental $B(E2)$ values (dots) and shell-model calculations (lines) of $T_z = -\frac{3}{2}$ (blue) and $+\frac{3}{2}$ (red) *sd* shell nuclei. The $(\frac{5}{2})^+ \to (\frac{1}{2})^+$ transition is shown in the top panel and the $(\frac{3}{2})^+ \to (\frac{1}{2})^+$ transition in the bottom panel.

For the $(\frac{5}{2})_1^+ \to (\frac{1}{2})_1^+$ transition four $B(E2)$ values for the neutron-rich nuclei exist and a first new data point is available for a neutron-deficient nucleus. The experimental data is in very good agreement with the shell-model calculations. More experimental data from the lighter proton-rich nuclei are needed to confirm the increasing deviation between mirror partners. The experimental information for the $(\frac{3}{2})_1^+ \to (\frac{1}{2})_1^+$ transition is even more limited. Only the data points for the $A = 33$ mirror pair exist. They agree with theoretical values within the uncertainties.

Another stringent comparison between experiment and shell model is enabled by isoscalar and isovector E2 matrix elements. The isoscalar and isovector MEs are extracted from $B(E2; 2_1^+ \to 0_1^+)$ values for $T = 1,2$ pairs and from $B(E2; \frac{5}{2_1}^+, \frac{3}{2_1}^+ \to \frac{1}{2_1}^+)$ values for $T = \frac{3}{2}$ pairs in the following way: $\mathrm{IS}(E2) = [B(E2;-T)^{1/2} + B(E2;+T)^{1/2}]/2$ and $\mathrm{IV}(E2) = [B(E2;-T)^{1/2} - B(E2;+T)^{1/2}]/2$. Shell model calculations were performed in the standard way with the modified USD interaction and polarization charge $\Delta e_{\pi,\nu} = 0.35e$.

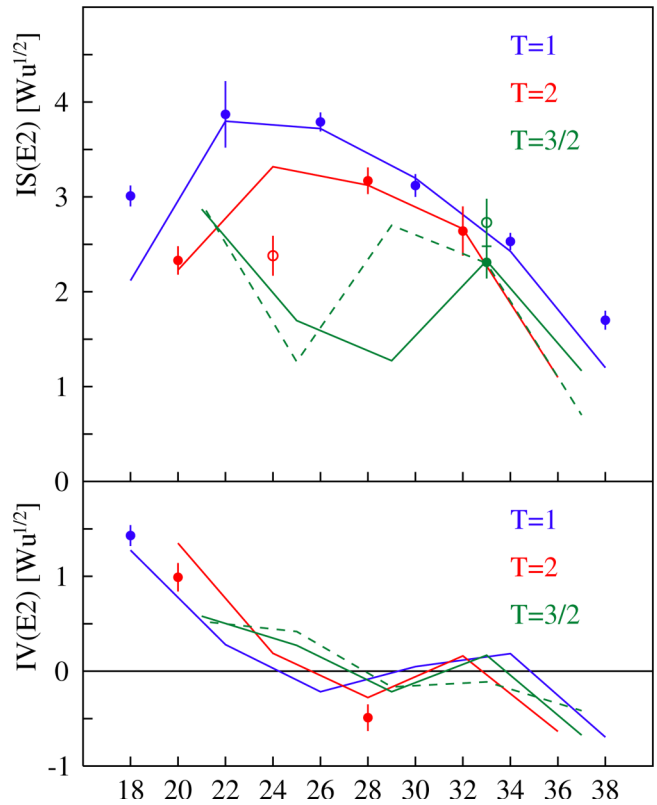

FIG. 8. (Color online) Experimental and shell-model (USD$^m_{2,3}$) isoscalar (IS, top) and isovector (IV, bottom) $E2$ transition matrix elements in *sd* shell nuclei. For $T = \frac{3}{2}$ only mirror pairs with odd-neutron $T_z = -T$ are considered, as the odd-proton nuclei are essentially proton unbound. The $T = \frac{3}{2}$ full and dashed lines refer to $(\frac{5}{2})^+ \to (\frac{1}{2})^+$ and $(\frac{3}{2})^+ \to (\frac{1}{2})^+$ transitions, respectively. For ^{33}P the averages of the two experimental results are listed in Table II, and for ^{22}Mg the more precise value of Ref. [33] is used.

In Fig. 8 the systematic of experimental and shell-model $E2$ matrix elements (MEs) for sd shell $T = 1,2,3/2$ nuclei is shown. For $T = 1,2$ both isoscalar and isovector MEs are well reproduced in the shell model. The deviations for the two-particle ($A = 18$) and two-hole ($A = 38$) $T = 1$ nuclei are due to the limitation of the model space, which does not allow for particle-hole excitations across the shell gap. The data point at the $A = 24$ pair suffers from the ^{24}Mg value, which may be either wrong as measured or incorrectly evaluated [28]. There are, however, three cases only where data are precise enough to extract the isovector ME. The $(2_1^+ \rightarrow 0_1^+)$ isoscalar values for $T = 1,2$ show a typical "collective" increase towards mid-shell and the asymmetry with respect to mid-shell is due to the fact that the $d_{5/2}^2$ and $d_{5/2}s_{1/2}$ MEs in the beginning of the shell are larger than the $d_{3/2}^2$ and $d_{3/2}s_{1/2}$ MEs at the end of shell. The $T = 3/2$ transitions show the expected single-particle features. The minima for $A = 25,29$ are due to the "magic" $Z,N = 14,16$ subshells. They should be sensitive to the USD$^m_{2,3}$ modifications. The isovector ME are all sensitive to shell and subshell structures, but effects are small and precision measurements are necessary. They are positive at the beginning of a shell ($T_z = -T$ are proton particles) and negative at the end ($T_z = -T$ are neutron holes). The ratio of IV/IS at the beginning and the end of the shell is therefore $\pm(e_\pi - e_\nu)/(e_\pi + e_\nu) = \pm\frac{1}{1.7}$.

Also for this comparison a more detailed validation of the shell-model predictions is needed, and measurements of other sd shell nuclei such as ^{21}Mg, ^{25}Si, or ^{29}S are suggested to be performed.

IV. SUMMARY

Experimental excitation energies and $B(E2)$ values of transitions in sd shell nuclei are compared to results of shell-model calculations employing isospin violating modifications of the USD interaction. The first experimental reduced transition strength values for the $T_z = -\frac{3}{2}$ nucleus ^{33}Ar were measured by means of relativistic Coulomb excitation. The effective interactions (USD$^m_{2,3}$) reproduce simultaneously the mirror-energy differences as well as the transition strengths in a wide range of $T_z = \pm 1, \pm\frac{3}{2}, \pm 2$ nuclei in the sd shell. Additional experimental data on transition strengths from light neutron-deficient sd shell nuclei are of highest interest to verify the predicted subshell structure as exhibited by the isoscalar $E2$ matrix elements.

ACKNOWLEDGMENTS

This work has been supported by the German BMBF under Contracts No. 05P09PKCI5, No. 05P12PKFNE, No. 05P09- RDFN4, and No. 05P12RDFN8; by Spanish Grants No. FPA2008-06419-C02-01 and No. FPA2011-24553; by the British STFC(UK); by the Swedish Research Council; by the Helmholtz International Center for FAIR (HIC for FAIR) funded by the State of Hesse; and by the Nuclear Astrophysics Virtual Institute (NAVI) funded by the Helmholtz Association. We acknowledge financial support from the Spanish Ministerio de Ciencia e Innovación under Contracts No. FPA2009-13377-C02 and No. FPA2011-29854-C04.

[1] P. Doornenbal *et al.*, Phys. Lett. B **647**, 237 (2007).
[2] A. Gade *et al.*, Phys. Rev. C **76**, 024317 (2007).
[3] A. P. Zuker, S. M. Lenzi, G. Martínez-Pinedo, and A. Poves, Phys. Rev. Lett. **89**, 142502 (2002).
[4] J. Ekman *et al.*, Phys. Rev. Lett. **92**, 132502 (2004).
[5] A. Brown and B. H. Wildenthal, Annu. Rev. Nucl. Part. Sci. **38**, 29 (1988).
[6] Y. Utsuno, T. Otsuka, T. Mizusaki, and M. Honma, Phys. Rev. C **60**, 054315 (1999).
[7] R. R. Reynolds *et al.*, Phys. Rev. C **81**, 067303 (2010).
[8] H. Nann *et al.*, Phys. Rev. C **9**, 1848 (1974).
[9] R. R. C. Clement *et al.*, Phys. Rev. Lett. **92**, 172502 (2004).
[10] C. E. Moss *et al.*, Phys. Rev. **174**, 420 (1968).
[11] E. H. Berkowitz *et al.*, Nucl. Phys. A **140**, 173 (1970).
[12] W. R. Harris *et al.*, Phys. Rev. C **2**, 1412 (1970).
[13] D. R. Goosman *et al.*, Phys. Rev. C **8**, 1324 (1973).
[14] P. Wagner *et al.*, Phys. Rev. C **7**, 2418 (1973).
[15] A. R. Poletti *et al.*, Phys. Rev. C **7**, 1433 (1973).
[16] R. Chakrabarti *et al.*, Phys. Rev. C **80**, 034326 (2009).
[17] H. Geissel *et al.*, Nucl. Instrum. Methods B **70**, 286 (1992).
[18] H. J. Wollersheim *et al.*, Nucl. Instrum. Methods A **537**, 637 (2005).
[19] J. Simpson *et al.*, Z. Phys. A **358**, 139 (1997).
[20] A. Maj *et al.*, Nucl. Phys. A **571**, 185 (1994).
[21] P. Golubev *et al.*, Nucl. Instrum. Methods A **723**, 55 (2013).
[22] R. Hoischen *et al.*, Nucl. Instrum. Methods A **654**, 354 (2011).
[23] A. Wendt, Ph.D. thesis, Universität Köln, 2013 (unpublished).
[24] C. A. Bertulani *et al.*, Comput. Phys. Commun. **152**, 317 (2003).
[25] J. Chen *et al.*, Nucl. Data Sheets **112**, 1393 (2011).
[26] N. Nica *et al.*, Nucl. Data Sheets **113**, 1 (2012).
[27] S. M. Perez, W. A. Richter, B. A. Brown, and M. Horoi, Phys. Rev. C **77**, 064311 (2008).
[28] ENSDF database, http://www.nndc.bnl.gov/ensdf/
[29] N. Iwasa *et al.*, RIKEN Accelerator Progress Report, 2005 (unpublished).
[30] P. D. Cottle *et al.*, Phys. Rev. Lett. **88**, 172502 (2002).
[31] S. Kanno *et al.*, Prog. Theor. Phys. (Kyoto) **146**, 575 (2002).
[32] Y. Togano *et al.*, Phys. Rev. Lett. **108**, 222501 (2012).
[33] H. Grawe, K. Holzer, and K. Kändler, Nucl. Phys. A **237**, 18 (1975).